Available online at www.sciencedirect.com
ScienceDirect
International Journal of Hydrogen Energy 32 (2007) 2273–2285
International Journal of HYDROGEN ENERGY
www.elsevier.com/locate/ijhydene

Light transfer in bubble sparged photobioreactors for H_2 production and CO_2 mitigation

Halil Berberoglu, Juan Yin, Laurent Pilon*

Mechanical and Aerospace Engineering Department, Henry Samueli School of Engineering and Applied Science, University of California, Los Angeles - Los Angeles, CA 90095, USA

Received 19 February 2007; accepted 20 February 2007
Available online 9 April 2007

Abstract

This paper presents a parametric study simulating light transfer in a photobioreactor containing gas bubbles and filamentous cyanobacteria *Anabaena variabilis* suspended in water. To the best of our knowledge, this paper presents for the first time a model for such system: (i) using a consistent set of radiation characteristics of the medium derived from experimental data and from Mie theory; (ii) accounting for anisotropic scattering by both the bubbles and the filamentous microorganisms; (iii) considering the spectral dependency of radiation characteristics in the spectral range from 400 to 700 nm using a box model, and (iv) evaluating light transfer in a photobioreactor containing genetically engineered microorganisms with reduced pigment content. The steady-state one-dimensional radiation transfer equation is solved using the modified method of characteristics and a quadrature with 24 directions per hemisphere adapted to forward scattering media. The parameters investigated include the bacteria concentration, the bubble radius, and the void fraction, as well as the approximate scattering phase function. It was established that the strongly forward scattering by the bubbles must be accounted for and the truncated phase function (TPF) is recommended. In the absence of bubbles, ignoring in-scattering by the bacteria leads to errors as high as 20%. On the other hand, accounting for in-scattering with isotropic phase function gives acceptable results. Moreover, genetically reducing the pigment content of the microorganisms by an order of magnitude increases the significance of forward scattering of light by the microorganisms. This in turn, increases the penetration depth and can be accounted for by either the Henyey–Greenstein or the TPF approximations. Finally, the model presented can also be applied to (i) other types of microorganisms such as unicellular green algae or photosynthetic bacteria, (ii) different photobioreactor processes such as food product or pharmaceutical production, or (iii) photochemical reactors.

Keywords: Photobiological hydrogen production; Carbon dioxide mitigation; Genetically modified bacteria; Reduced pigment; Algae; Cyanobacteria; Bubble column; Airlift; Photobioreactor; Light transfer; Modeling

1. Introduction

Increased amounts of greenhouse gas emissions as well as the exhaustion of inexpensive and accessible fossil fuel resources are calling for clean and renewable energy sources. Hydrogen, to be used in fuel cells, is considered to be an attractive alternative fuel since water vapor is the only byproduct from its reaction with oxygen. Photobiological hydrogen production by cultivation of cyanobacteria (or green algae) offers a clean and sustainable alternative to thermochemical or electrolytic production technologies.

During photobiological hydrogen production, light from the sun is absorbed by microorganisms such as algae, cyanobacteria or photosynthetic bacteria to produce hydrogen [1]. The reader is referred to Refs. [1–6] for detailed reviews of photobiological hydrogen production. In particular, the cyanobacterium *Anabaena variabilis* has been studied extensively and identified as a good candidate for hydrogen production [7]. Therefore, it is chosen as the microorganism of interest in the present study.

The cyanobacterium *A. variabilis* is a photosynthetic prokaryote which uses CO_2 as its carbon source, water as its electron source, and sunlight as its energy source. Fig. 1 (a) shows a micrograph of a filament of *A. variabilis*, approximately 5 μm in diameter and 100 μm in length, composed of vegetative cells and heterocysts. It uses the light energy in the

* Corresponding author. Tel.: +1 310 206 5598; fax: +1 310 206 4830.
E-mail address: pilon@seas.ucla.edu (L. Pilon).

0360-3199/$ - see front matter © 2007 International Association for Hydrogen Energy. Published by Elsevier Ltd. All rights reserved.
doi:10.1016/j.ijhydene.2007.02.018

Nomenclature

A_i	interfacial area concentration, m^2/m^3
a	bubble radius, m
$A_{abs,\lambda}$	spectral mass absorption cross-section of microorganisms, m^2/kg
D	dilution factor
$S_{sca,\lambda}$	spectral mass scattering cross-section of microorganisms, m^2/kg
f_1	weighing factor in TPF
f_B	void fraction
G	irradiance, W/m^2
g	asymmetry factor
h_1	weighing factor in TPF
I	light intensity, $W/m^2/sr$
k	absorption index
n	index of refraction
$Q_{sca,B}$	scattering efficiency of the bubbles
r_X	radius of microorganisms
$\vec{s}$	unit vector into a given direction
v_X	specific volume of the microorganisms, m^3/kg
w_i	weighting factors of the Gaussian quadrature
X	microorganism concentration, kg dry cell/m^3
z	distance from the illuminated surface, m

Greek symbols

β	extinction coefficient, m^{-1}
θ	polar angle, rad
θ_i	discrete polar angles corresponding to the directions of the Gaussian quadrature, rad
Θ	angle between incident and scattered directions, rad
κ	absorption coefficient, m^{-1}
λ	wavelength, nm
λ_c	box center wavelength, nm
σ	scattering coefficient, m^{-1}
ϕ	azimuthal angle, rad
Φ	scattering phase function
χ	size parameter
Ω	solid angle, sr
ω_{eff}	average single scattering albedo

Subscripts

abs	refers to absorption
in	refers to incident radiation
D	refers to the dilution factor
w	refers to water
X	refers to bacteria or bacteria concentration
λ	refers to wavelength
HG	refers to Henyey–Greenstein phase function
PAR	refers to photosynthetically active radiation ($400\,nm \leqslant \lambda \leqslant 700\,nm$)
TPF	refers to truncated phase function
sca	refers to scattering

spectral range from 400 to 700 nm, known as the photosynthetically active radiation (PAR). In turn, it produces biomass (i.e., it multiplies), as well as oxygen and hydrogen. In addition, *A. variabilis* is capable of fixing molecular nitrogen present in air using the enzyme nitrogenase [5]. As part of its nitrogen fixation metabolism, it generates hydrogen as a byproduct [5]. In the absence of molecular nitrogen, hydrogen production by the nitrogenase enzyme is promoted [5]. However, the functioning of nitrogenase, both for fixing nitrogen and producing hydrogen, is inhibited by the dissolved oxygen in the growth medium [8]. In addition, *A. variabilis* also possesses the enzyme uptake hydrogenase which consumes hydrogen to reduce molecular oxygen [5].

Dissolved oxygen accumulation, limited light penetration, and carbon dioxide availability to the microorganisms are the major factors affecting the performance of a photobioreactor for the production of hydrogen [2]. Researchers are trying to overcome these limitations by genetically engineering microorganisms and designing novel photobioreactors [7,9,10]. For example, *A. variabilis* has been genetically modified to lack the hydrogen consuming enzyme uptake hydrogenase [11–13]. The mutant forms had 3–4.3 times higher hydrogen production rates compared with the wild forms. In addition, Melis et al. [10,14] reduced the pigment content of the green algae *Dunaliella salina* from 1×10^9 Chlorophyll molecules per cell (Chl/cell) to 0.15×10^9 Chl/cell for overcoming the light penetration problem in large photobioreactors. More recently, Polle et al. [15] genetically engineered the green algae *Chlamydomonas reinhadtii* to have a truncated light harvesting chlorophyll antenna size. The authors reported that the microorganisms with less pigments had higher quantum yield, photosynthesis rate, and light saturation irradiance. In addition, Melis et al. [6,10] showed that pure hydrogen production can be achieved by *C. reinhadtii* under sulfur deprivation. The authors stated that with this method photosynthetic oxygen production is slowed down and pure hydrogen is produced by the culture, overcoming the oxygen inhibition of the hydrogen producing enzymes, as well as eliminating the dangerous mixtures of hydrogen and oxygen. As an alternative, Greenbaum et al. [16] experimentally showed that the inhibitory effect of molecular oxygen on hydrogen production can be alleviated by having a headspace volume three time that of the liquid phase which ensures low dissolved oxygen concentration in the bacteria medium. By having a large headspace volume, the molar fraction of oxygen is kept low in the gas phase which ensures more oxygen to partition into the gas phase. This approach can

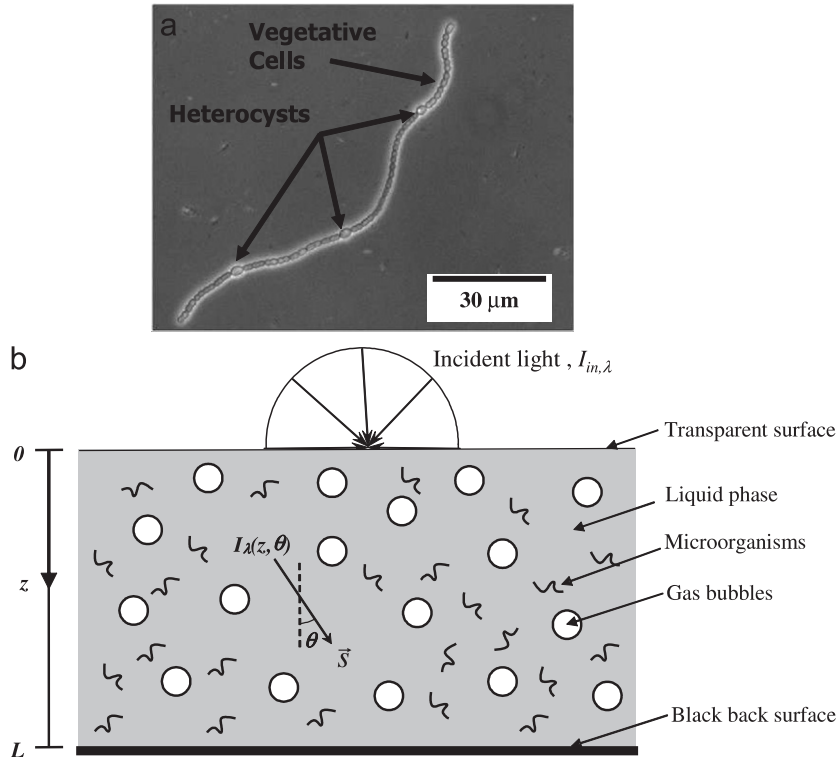

Fig. 1. (a) Micrograph of *A. variabilis*; (b) schematic of the photobioreactor system considered.

be improved and the mass transfer limitations, including limited CO_2 transfer, oxygen, and hydrogen accumulation, can be alleviated by sparging the photobioreactor with bubbles. Moreover, sparging with bubbles enables relatively inexpensive and effective mixing within the photobioreactor that is necessary to avoid settling of the microorganisms. Furthermore, even in absence of bubble sparging, during photobiological hydrogen production, small bubbles of hydrogen and oxygen are generated in the photobioreactor due to bacterial activity. However, the presence of bubbles affects the light transfer within the photobioreactor. Therefore, it is necessary to model and analyze the effects of the presence of both bubbles and microorganisms (wild strain or genetically modified) on light transfer in order to optimize the design, scale-up, and operation of hydrogen producing photobioreactors.

Pioneering work in simulating light transfer in micro-algal ponds was published by Daniel et al. [17]. The authors used the radiative transport equation (RTE) on a gray basis and accounted only for the presence of unicellular algae. They estimated the scattering phase function of unicellular algae with a weighted sum of thirty Legendre polynomials to be used in solving the RTE. They recommended using the six-flux approximation for solving the RTE. Moreover, they concluded that scattering is unimportant when the single scattering albedo is less than 0.5 and scattering is strongly in the forward direction. Moreover, Kim et al. [18] modelled light transfer in a sulfate reducing photobioreactor using Beer–Lambert's law. The authors used an effective extinction coefficient accounting for light absorption by bacteria and light scattering by the sulphur crystals they excrete. In addition, Cornet et al. [19–21] applied the RTE to model the light transfer for cultivating filamentous cyanobacterium *Spirulina platensis* accounting for absorption and *isotropic* scattering by the microorganisms. The absorption and scattering coefficients of the microorganisms were obtained from experimental data. The RTE was solved using the Schuster–Schwarzschild two-flux approximation. Their model ignored the strongly forward scattering of a fibrous medium [22]. Finally, none of the above mentioned studies accounted for the spectral dependency of the radiation characteristics.

Recently, Merzlyak and Naqvi [23] utilized an integrating sphere and the analysis method proposed by Latimer and Eubanks [24] to measure the spectral absorption and scattering coefficients of *A. variabilis* in the range from 350 to 750 nm. The authors assumed that the scattering phase function was independent of wavelength in the PAR. In addition, Stramski and Mobley [25] measured experimentally the spectral refractive index, absorption index, phase function, absorption and scattering cross-section of the cyanobacteria *Synechococcus* using Mie theory for spherical scatterer over the spectral range from 350 to 750 nm. Their results corroborate the assumption of Merzlyak and Naqvi [23] that the scattering phase function of cyanobacteria is independent of wavelength in the PAR and establish that it is strongly forward. More recently, Pottier et al. [26] determined the spectral radiative characteristics of *C. reinhardtii* from Mie theory for spherical scatterers and computed the complex index of refraction of bacteria using reported pigment concentration and optical properties. The authors solved the RTE in the PAR with a spectral resolution of 1 nm using the

Schuster–Schwarzschild two-flux approximation. Anisotropic scattering was accounted for through the back-scattered fraction which was small for these type of bacteria. Finally, they validated their results with experimental measurements of the total irradiance in the PAR along the depth of the photobioreactor. The authors acknowledged that for more complex bacteria shapes (e.g. cylinders and spheroids), more sophisticated numerical tools are required to predict radiative properties and calculate light distribution. In addition, they did not consider the presence of other scatterers such as bubbles in the photobioreactor.

The objective of this study is to simulate light transfer in a bubble sparged photobioreactor in order to maximize hydrogen production and carbon dioxide consumption. *A. variabilis* is used for illustration purposes and since its radiation characteristics are known [23]. The analysis presented here aims at modeling and simulating light transfer within a bubble sparged photobioreactor for various filamentous microorganism concentrations, bubble radius, and void fractions accounting for absorption and anisotropic scattering over the spectral range from 400 to 700 nm. Approximations for the bacteria phase function are discussed in details. In addition, genetically engineered microorganisms with reduced pigment content are also considered.

2. Analysis

Let us consider a plane-parallel photobioreactor as shown schematically in Fig. 1(b). The reactor contains the cyanobacterium *A. variabilis* at concentration X with respect to the total volume of the reactor expressed in kg dry cell/m^3, and bubbles with radii a and void fraction f_B offering large gas/liquid interfacial area for mass transfer. The microorganism concentration X ranges from 0.035 to 0.35 kg dry cell/m^3. The bubble radius a ranges from 25 to 150 μm offering higher interfacial area than millimeter size bubbles for the same void fraction, thus increasing the mass transfer rate. Finally, the void fraction is such that $0 \leqslant f_B \leqslant 0.3$ so bubbly flow prevails [27]. The reactor is considered to be illuminated only from the top with diffuse intensity I_{in}. As the light penetrates into the photobioreactor, it is absorbed by the liquid phase and by the microorganisms and scattered anisotropically by both the bubbles and the microorganisms.

2.1. Assumptions

In order to make the problem mathematically trackable the following assumptions are made:

1. Light transfer is one-dimensional.
2. Steady-state radiation transfer prevails.
3. The microorganisms, and the bubbles are uniformly distributed in the reactor.
4. The bubbles and microorganisms are monodisperse.
5. The liquid phase is cold, absorbing, and non-scattering.
6. The optical properties of the liquid phase are those of pure water.
7. The gas bubbles are non-absorbing but only scattering.
8. The phase function of the bubbles is computed from Mie theory assuming the liquid phase is non-absorbing and the bubbles are spherical.
9. The scattering phase function of the filamentous microorganisms is that of a medium consisting of infinitely long fibers embedded in water and computed from Mie theory. They are assumed to be randomly oriented due to the agitation created by mechanical stirring or by the rising bubbles.
10. Independent scattering prevails for both the microorganisms and the bubbles. Studies by Tien and Drolen [28], and Lee [29] confirm this assumption for the ranges of parameters under consideration.
11. The photobioreactor's top surface is non-reflecting.

2.2. Governing equations

The RTE is an energy balance on the radiative energy traveling in a particular direction $\vec{s}$. Considering the in-scattering by microorganisms and bubbles separately, the one-dimensional steady-state RTE can be written as

$$\vec{s}\cdot\frac{\partial I_\lambda(z,\vec{s})}{\partial z} = -\kappa_{\mathrm{eff},\lambda} I_\lambda(z,\vec{s}) - \sigma_{\mathrm{eff},\lambda} I_\lambda(z,\vec{s}) + \frac{\sigma_{X,\lambda}}{4\pi}\int_{4\pi} I_\lambda(z,\vec{s}_i)\Phi_{X,\lambda}(\vec{s}_i,\vec{s})\,\mathrm{d}\Omega_i + \frac{\sigma_{B,\lambda}}{4\pi}\int_{4\pi} I_\lambda(z,\vec{s}_i)\Phi_{B,\lambda}(\vec{s}_i,\vec{s})\,\mathrm{d}\Omega_i, \quad (1)$$

where $I_\lambda(z,\vec{s})$ is the radiation intensity in direction $\vec{s}$ at location z, and $\kappa_{\mathrm{eff},\lambda}$ and $\sigma_{\mathrm{eff},\lambda}$ are the effective spectral absorption and scattering coefficients, respectively. The coefficients $\sigma_{X,\lambda}$ and $\sigma_{B,\lambda}$ are the spectral scattering coefficients of the microorganisms and the bubbles, respectively. The scattering phase functions of bacteria and bubbles, are denoted by $\Phi_{X,\lambda}$ and $\Phi_{B,\lambda}$, respectively. They describe the probability that radiation traveling in the solid angle $\mathrm{d}\Omega_i$ around the direction $\vec{s}_i$ will be scattered into the solid angle $\mathrm{d}\Omega$ around direction $\vec{s}$. The effective absorption coefficient $\kappa_{\mathrm{eff},\lambda}$ accounts for the absorption by the liquid phase and by the microorganisms at wavelength λ. It can be written in terms of the void fraction f_B and of the microorganism concentration X,

$$\kappa_{\mathrm{eff},\lambda} = \kappa_{L,\lambda}(1 - f_B - X v_X) + A_{\mathrm{abs},\lambda} X, \quad (2)$$

where v_X is the specific volume of cyanobacteria equal to 0.001 m^3/kg. The absorption coefficient of the liquid phase $\kappa_{L,\lambda}$ is expressed in m^{-1}, and the mass absorption cross-section of microorganisms $A_{\mathrm{abs},\lambda}$ is expressed in m^2/kg. The term $\kappa_{X,\lambda} = A_{\mathrm{abs},\lambda} X$ corresponds to the absorption coefficient of microorganisms. Finally, the term $X v_X$ represents the volume fraction of photobioreactor occupied by microorganisms and has a maximum value of 3.5×10^{-4}.

Assuming independent scattering, the effective scattering coefficient of the composite medium $\sigma_{\mathrm{eff},\lambda}$ can be expressed as the sum of the scattering coefficients of the microorganisms

Table 1
Summary of the optical properties of wild strain *A. variabilis* ATCC 29413-U and boundary conditions for each box

Box	Wavelength	Liquid phase		Bubbles	Microorganisms				B.C.
	λ_c (nm)	n_{L,λ_c}	κ_{L,λ_c} ($\times 10^3$ m^{-1})	$Q_{sca,B}$	n_{X,λ_c}	k_{X,λ_c} $\times 10^3$	A_{abs,λ_c} (m^2/kg)	S_{sca,λ_c} (m^2/kg)	I_{in,λ_c} (Wm^{-2}sr^{-1})
1	434	1.33	35.9	1.0	1.41	10.09	423.68	68.82	5.44
2	512	1.33	30.9	1.0	1.41	6.37	209.91	68.74	7.22
3	627	1.33	283.4	1.0	1.41	2.73	319.91	63.57	10.69

$\sigma_{X,\lambda}$ and of the bubbles $\sigma_{B,\lambda}$ as

$$\sigma_{eff,\lambda} = \sigma_{X,\lambda} + \sigma_{B,\lambda} = S_{sca,\lambda} X + (3 f_B/4a) Q_{sca,B}(a, \lambda), \quad (3)$$

where $S_{sca,\lambda}$ is the mass scattering cross-section of microorganisms expressed in m^2/kg and $Q_{sca,B}(a, \lambda)$ is the scattering efficiency factor of monodispersed bubbles of radius a at wavelength λ obtained from Mie theory. Note that $3 f_B/a$ is the interfacial area concentration A_i of the bubbles and $\sigma_{B,\lambda}$ can alternatively be written as

$$\sigma_{B,\lambda} = (A_i/4) Q_{sca,B}(a, \lambda). \quad (4)$$

Finally, the reactor is illuminated with a diffuse light source only from the top and the back surface is assumed to be cold and black. Therefore, the boundary conditions for Eq. (1) can be written as

$$I_\lambda(0, \theta) = I_{in,\lambda} \quad \text{for } 0 \leqslant \theta < \pi/2,$$
$$I_\lambda(L, \theta) = 0 \quad \text{for } \pi/2 < \theta < \pi, \quad (5)$$

where I_λ is the intensity of sunlight at λ. The Sun is assumed to be a blackbody at temperature 5800 K and the total irradiance incident on the photobioreactor denoted by $G_{PAR,in}$, is equal to 146.71 W/m^2 in the PAR [30] and defined as

$$G_{PAR,in} = 2\pi \int_{400}^{700} I_{in,\lambda}\, d\lambda = 146.71\ \text{W/m}^2. \quad (6)$$

2.3. Closure laws

The values of the radiation characteristics associated with the liquid phase, the microorganisms, and the bubbles approximated with the box model [30] are summarized in Table 1and are discussed in the following sections.

2.3.1. The microorganisms

In order to simplify the numerical simulations, the PAR is divided in three sections where the spectral quantities needed to solve Eq. (1) are estimated using the box model [30]. This model approximates the spectral absorption and scattering coefficients with a series of boxes of width $\Delta\lambda$ and height κ_{X,λ_c} and σ_{X,λ_c}, respectively, centered around the wavelength λ_c such that the area under the original spectrum equals the area under the box [30]. Here, the absorption and scattering spectrum of *A. variabilis* is approximated using three boxes with wavelength intervals from 400 to 469, 469 to 556, and 556 to 700 nm. The center wavelengths of the boxes are assigned at the midpoint of each box, namely at 434, 512, and 627 nm. Fig. 2 reproduces the reported spectral absorption and scattering coefficients of *A.variabilis* reported by Merzlyak and Naqvi [23] along with

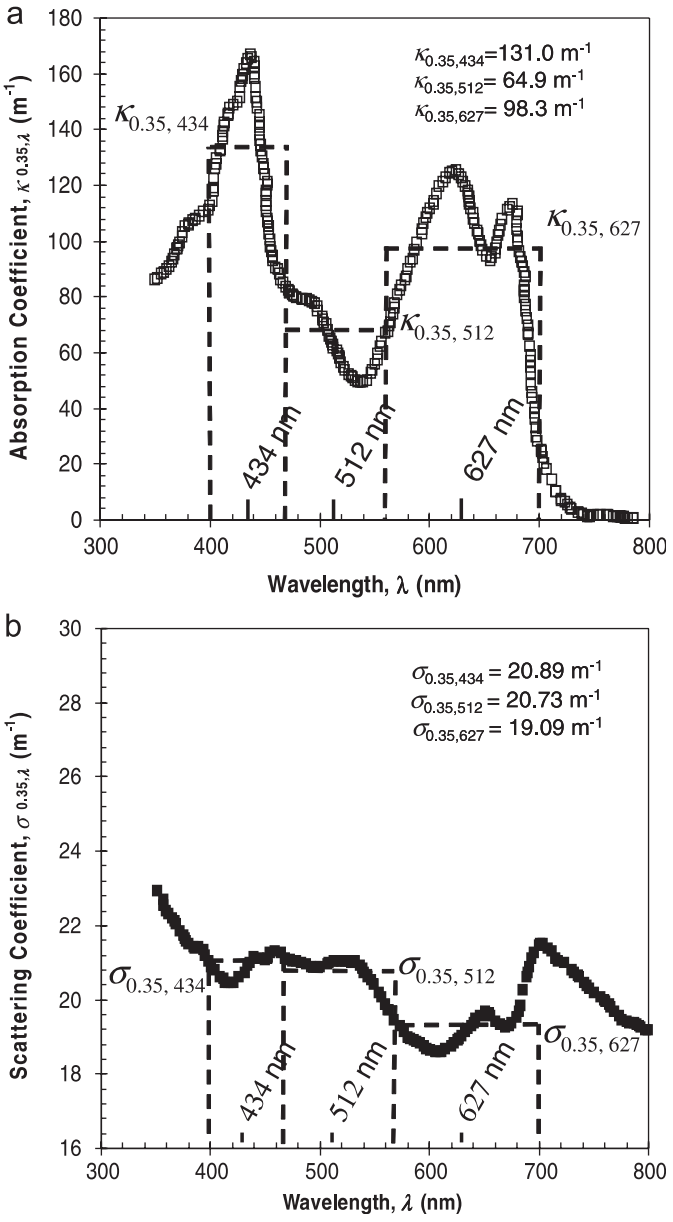

Fig. 2. The box model applied to the (a) absorption and (b) scattering coefficients of *A. variabilis* at concentration $X = 0.35$ kg dry cell/m^3 in the photosynthetically active part of the spectrum [23].

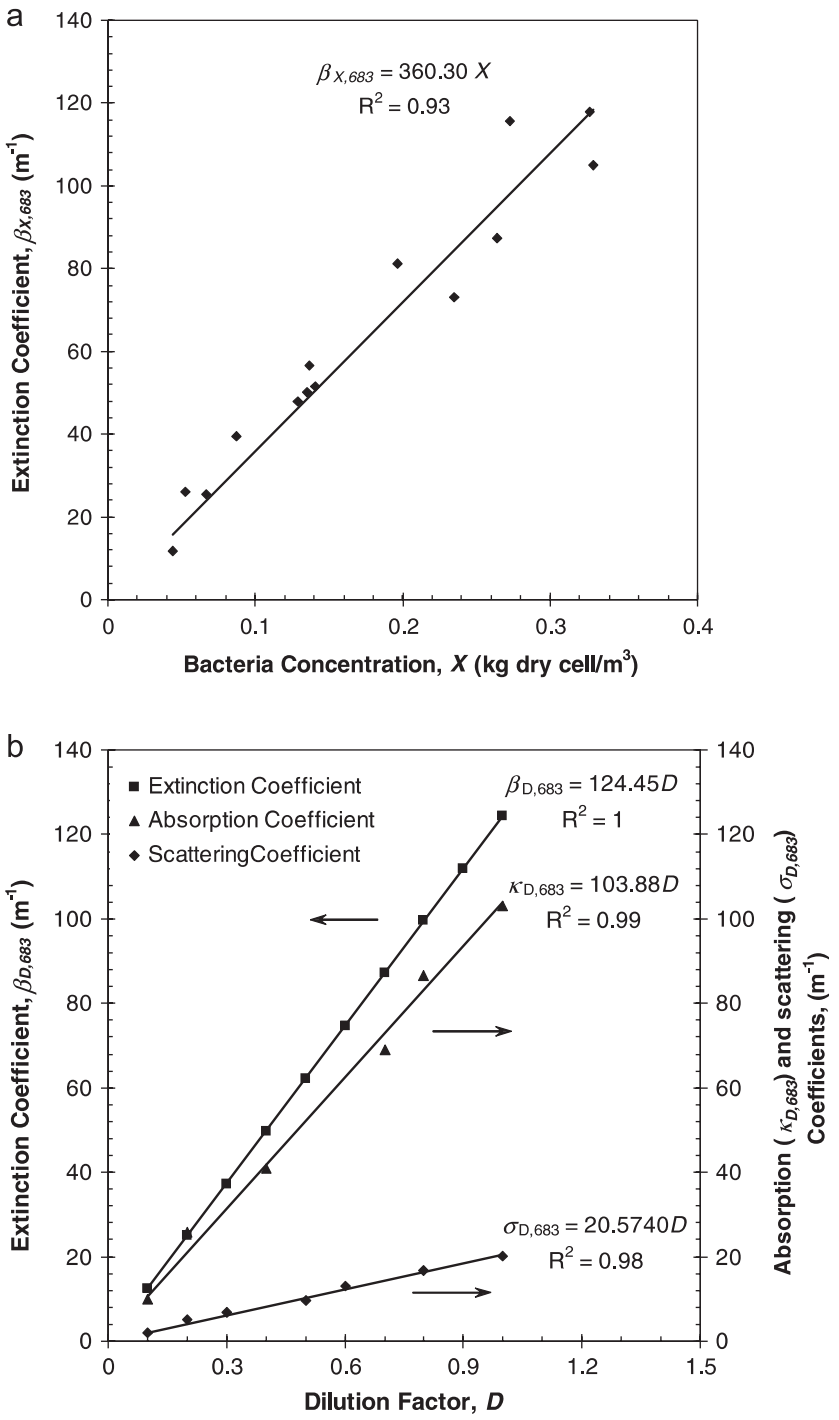

Fig. 3. (a) Calibration curve for the extinction coefficient of *A. variabilis* at 683 nm against bacteria concentration, (b) extinction coefficient of *A. variabilis* at 683 nm against the dilution factor [23].

the three boxes. Boxes 1 and 3 capture the absorption peaks of the pigment chlorophyll *a* which is responsible for absorbing sun light and providing energy for photosynthesis and hydrogen production. Merzlyak and Naqvi [23] reported the absorption and scattering coefficient data as a function of the dilution factor D defined as the normalized bacteria concentration with respect to the unreported maximum bacteria concentration $X_{\max}$ used in their experiments, i.e., $D = X/X_{\max}$. In order to utilize the data reported by Merzlyak and Naqvi [23], the relationship between D and X must be found. This is achieved by comparing the extinction coefficient $\beta_{X,\lambda}$, obtained as a function of X from calibration experiments performed in our laboratory using a spectrophotometer (Cary-3E by Varian, USA), to the extinction coefficient $\beta_{D,\lambda}$ reported as a function of D [23]. The calibration experiments are conducted at wavelength 683 nm and at 13 different bacteria concentrations covering the

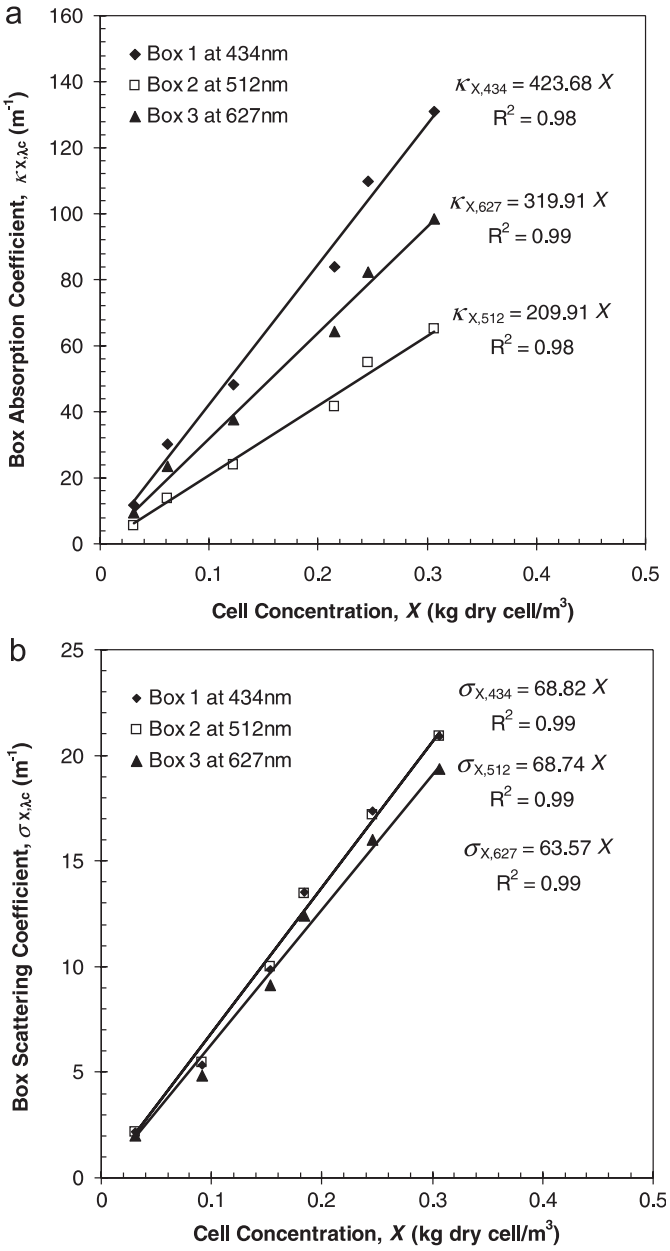

Fig. 4. Variations of (a) the three box absorption κ_{X,λ_c} and (b) the scattering coefficients σ_{X,λ_c} as functions of bacteria concentrations X [23].

range from 0.04 to 0.35 kg/m^3. Fig. 3(a) shows that $\beta_{X,683}$ is directly proportional to X and such that $\beta_{X,683} = 360.30X$. The relationship between D and $\beta_{D,683}$ is obtained by summing the slopes of the absorption and scattering coefficients given by Merzlyak and Naqvi [23] as reproduced in Fig. 3(b). This relationship can be summarized as $\beta_{D,683} = 124.45D$. Comparing the two equations establishes that $D = 2.90X$ or $X_{\max} = 0.35$ kg dry cell/m^3.

Moreover, the absorption and scattering coefficients of *A. variabilis* for each box are calculated for various microorganism concentrations and presented in Fig. 4. It shows that both absorption and scattering coefficients are linearly proportional to the microorganism concentration X. The slopes of these curves correspond to the mass absorption A_{abs,λ_c} and scattering S_{sca,λ_c} cross-sections of *A. variabilis* for a given box centered around λ_c. The scattering cross-section of *A. variabilis* in boxes 1 and 2 do not differ appreciably as shown in Fig. 4(b).

Finally, the scattering phase function of *A. variabilis* is assumed to be that of randomly oriented infinitely long fibers embedded in water [Assumption (9)]. The code implementing Mie theory for normally incident radiation on a single infinitely long cylinder was given by Bohren and Huffman [31]. This code has been modified to calculate the scattering phase function of a medium of randomly oriented infinitely long cylinders and has been successfully validated against the results reported by Lee [22]. The absorption index of water is on the order of 10^{-9} and taken as zero while its refractive index is taken as 1.33. The values of the refractive index in each box n_{X,λ_c} and of the absorptive index k_{X,λ_c} of bacteria, are obtained from Stramski and Mobley [25] and are reported in Table 1. The results of Mie theory indicate that the scattering phase function does not change appreciably over the spectral range of interest and for the size parameter of microorganisms χ_X between 22 and 39, where χ_X is defined in terms of the filamentous microorganism radius r_X as $\chi_X = 2\pi r_X/\lambda$ with $r_X = 5\,\mu$m.

Alternatively, the microorganism phase function can be approximated as a Henyey–Greenstein (HG) phase function. The asymmetry factor $g_X = 0.9919$ was computed using the results of Mie theory according to $g_X = \int_{4\pi} \Phi_X(\Theta)\cos(\Theta)\,d\Omega/4\pi$. The phase function can also be expressed as a truncated phase function (TPF). In this second model, $\Phi(\Theta)$ is divided in two parts, from 0 to Θ_{cutoff} and from Θ_{cutoff} to π. Each part is a linear combination of two HG phase functions with asymmetry factors $g_{\text{TPF},1}$, and $g_{\text{TPF},2}$. The TPF is expressed as

$$\Phi(\Theta) = f_1\Phi_{\text{HG},g_{\text{TPF},1}}(\Theta) + (1-f_1)\Phi_{\text{HG},g_{\text{TPF},2}} \quad \text{for } 0 \leqslant \Theta \leqslant \Theta_{\text{cutoff}},$$

$$\Phi(\Theta) = h_1[f_1\Phi_{\text{HG},g_{\text{TPF},1}}(\Theta) + (1-f_1)\Phi_{\text{HG},g_{\text{TPF},2}}] \quad \text{for } \Theta_{\text{cutoff}} < \Theta < \pi, \tag{7}$$

where f_1 and h_1 are weighing parameters. The parameters f_1, h_1, Θ_{cutoff}, $g_{\text{TPF},1}$, and $g_{\text{TPF},2}$ are determined by minimizing the sum of the squares of the error between Mie theory calculations and the TPF model. The parameters are found to be $f_1 = 0.104$, $h_1 = 0.4$, $\Theta_{\text{cutoff}} = \pi/3$, $g_{\text{TPF},1} = 0.99997$, and $g_{\text{TPF},2} = 0.992$ for all the wavelengths in the PAR. Finally, Eq. (7) is normalized by the method previously adopted by Nicolau et al. [32]. Fig. 5(a) shows the phase functions of *A. variabilis* calculated by: (i) Mie theory; (ii) the HG phase function and (iii) the TPF corresponding to $\lambda_c = 512$ nm and size parameter $\chi_X = 30$. One can see that the HG phase function over-predicts the backscattering, the scattering phase function for $\Theta > 90°$, whereas the TPF provides a more accurate approximation of Mie theory results.

2.3.2. The bubbles

The scattering efficiency factor $Q_{\text{sca,B}}(a,\lambda)$ and the scattering phase function $\Phi_B(\Theta)$ of the bubbles are predicted by Mie theory using the code provided by Bohren and Huffman [31] applied to a sphere of radius a and refractive index 1 embedded in water with $n_L = 1.33$. The results indicate that

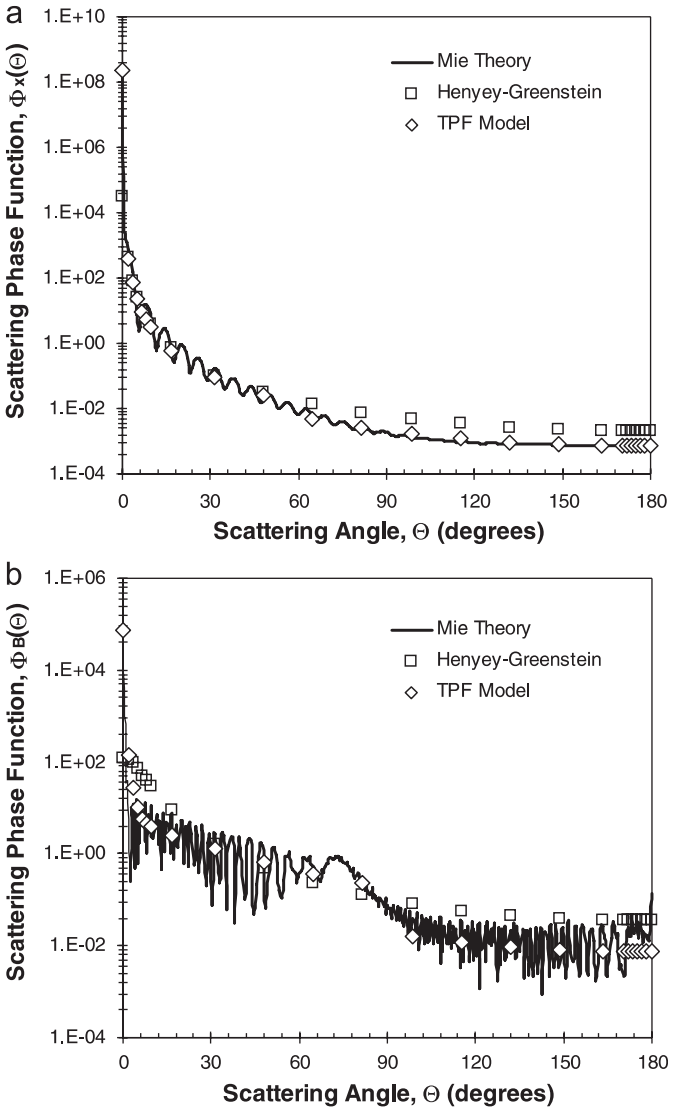

Fig. 5. Comparison of the exact and approximate phase functions at wavelength $\lambda_C = 512\,\text{nm}$ for (a) *A. variabilis* with $\chi_X = 30$ and (b) a bubble of size parameter $\chi_B = 1500$ in water.

$Q_{\text{sca,B}}(a, \lambda)$ is equal to 1.0 (corrected for the diffraction paradox) and does not vary more than 0.4% for the bubble size parameter $\chi_B = 2\pi a/\lambda$ such that $224 \leqslant \chi_B \leqslant 2356$ in the PAR with a between 25 and 150 μm. Therefore, the scattering coefficient for the bubbles is independent of the wavelength and can be written as, $\sigma_{B,\lambda} = 0.75 f_B/a$. In addition, it was found that $\Phi_B(\Theta)$ is strongly forward and does not vary appreciably for the size parameters considered. Moreover, in order to simplify the calculations, the phase function obtained from Mie theory is approximated by the HG phase function with a computed asymmetry factor equal to $g_B = 0.8768$. Alternatively, $\Phi_B(\Theta)$ can be estimated by the TPF with parameters $f_1 = 0.6$, $h_1 = 0.1$, $\Theta_{\text{cutoff}} = \pi/2$, $g_{\text{TPF},1} = 0.996$, and $g_{\text{TPF},2} = 0.55$. Fig. 5(b) compares the phase functions obtained by: (i) Mie theory; (ii) the HG phase function, and (iii) the TPF for a bubble of size parameter $\chi_B = 1500$ at wavelength $\lambda = 512\,\text{nm}$. Here also the HG phase function over predicts the back-scattering while the TPF provides a better approximation of Mie theory results.

2.3.3. The liquid phase

The values of refractive and absorption indices of water are obtained from Ref. [33] and approximated with the box model. The refractive index of water, $n_{L,\lambda}$ remains relatively constant and equal to 1.33 throughout the PAR. The absorption coefficient of water $\kappa_{L,\lambda}$ is proportional to the absorption index of water $k_{L,\lambda}$ and defined as $\kappa_{L,\lambda} = 4\pi k_{L,\lambda}/\lambda$. As presented in Table 1, the maximum value of $\kappa_{L,\lambda}$ is $0.283\,\text{m}^{-1}$ which is an order of magnitude smaller than the absorption coefficient of microorganisms at their lowest concentration $X = 0.035\,\text{kg dry cell/m}^3$.

2.4. Method of solution

The modified method of characteristics [34] is employed to solve Eq. (1). It consists of transforming a hyperbolic partial differential equation into a set of ordinary differential equations (ODEs) which are solved along the characteristic curves of the photons. It makes use of an arbitrary set of points and traces photons backward in space from each point. The integral for the in-scattering term is computed using the discrete ordinate method with a combination of two Gauss quadrature having 24 discrete directions $(\Theta_i)_{1 \leqslant i \leqslant 24}$ per hemisphere along with the associated weighting factors w_i successfully used by Baillis et al. [35,36] for strongly forward scattering fused quartz containing bubbles. Then, the ODEs are solved using the fourth order Runge–Kutta method at every point. Finally, the local spectral irradiance (or fluence) is defined as

$$G_{\lambda_c}(z) = \int_{4\pi} I_{\lambda_c}(z, \vec{s})\,\mathrm{d}\Omega = 2\pi \sum_{i=1}^{24} w_i\, I_{\lambda_c}(z, \theta_i) \tag{8}$$

and computed similarly using the discrete ordinate method. The local spectral irradiance calculated for each of the three boxes are added to give the total local irradiance in the PAR as

$$G_{\text{PAR}}(z) = G_{434}(z) + G_{512}(z) + G_{627}(z). \tag{9}$$

The total local irradiance $G_{\text{PAR}}(z)$ can then be used to model the bacterial growth, carbon dioxide consumption, and hydrogen and oxygen production.

Finally, a grid sensitivity study was performed to make sure that the computed values of $G_{\text{PAR}}(z)$ were independent of the grid size. To do so, the number of grid points was doubled until $G_{\text{PAR}}(z)$ did not change by more than 1%. It was found that 1200 points along the z-direction satisfied this criterion for all bubble and bacteria concentrations explored. The CPU time was 3.7 min for isotropic scattering and low bacteria concentration without bubbles and 4.1 min for TPF with the largest bacteria and bubble interfacial area concentrations, for example with an Intel Celeron(R) CPU of 2.93 GHz and 504 MB RAM.

3. Results and discussion

Simulations have been performed for low ($X = 0.035\,\text{kg/m}^3$) and high ($X = 0.35\,\text{kg/m}^3$) microorganism concentrations at

three different interfacial area concentrations A_i $(=3f_B/a)$ namely 0, 450, and 1500 m^{-1}. The total local irradiance $G_{PAR}(z)$ has been calculated for each combination of bacteria and interfacial area concentrations with four different approaches: (1) neglecting the in-scattering term; (2) assuming isotropic scattering for bubbles and microorganisms; (3) accounting for anisotropic scattering by both scatterers using the HG phase function, and (4) the TPF. To assess the overall contribution of the scattering to extinction, the average single scattering albedo over the PAR is calculated as

$$\omega_{\text{eff}} = \frac{\sum_{\text{box }1}^{3} \sigma_{\text{eff},\lambda_c}}{\sum_{\text{box }1}^{3} (\sigma_{\text{eff},\lambda_c} + \kappa_{\text{eff},\lambda_c})}. \quad (10)$$

The results for the total local irradiance $G_{PAR}(z)$ normalized by the total incident irradiance, $G_{PAR,in} = 146.71\ W/m^2$, are presented in Fig. 6. For the sake of clarity results within the first 20 mm are presented for high bacteria concentrations. Since the objective of the study is to determine the availability of light to microorganisms in the photobioreactor and to facilitate effective comparison of the results, the penetration depth is arbitrarily defined as the distance from the illuminated surface at which the total irradiance $G_{PAR}(z)$ decreases below 20% of $G_{PAR,in}$. The penetration depths obtained assuming isotropic scattering, ignoring in-scattering, and accounting for anisotropic scattering are reported in Table 2.

First, results from the three box model were compared with spectral calculations with a wavelength increment $\Delta\lambda$ of 1 nm over the PAR and for bacteria concentration $X = 0.35\ kg/m^3$ without bubbles. It is found that the box method is about 71 times faster than the spectral calculation and underestimates the penetration depth by 9.8% and the total fluence by a maximum of 1.52 W/m^2 (5.8%). Finally, the box method overestimates the total fluence at $z = 0$ by 0.02%. This justifies the use of the proposed box model which gives acceptable results for a much faster computation.

Figs. 6(a) and (b) compare the four models for scattering by the microorganisms in the absence of bubbles in the photobioreactor for low and high bacteria concentrations, respectively. They indicate that the computed penetration depth assuming isotropic scattering by microorganisms does not differ more than 6% from the case when anisotropic scattering is accounted for. However, ignoring in-scattering, as in the case of Beer–Lambert's law, gives relative difference as high as 20% for the penetration depth with respect to the anisotropic scattering case. On the other hand, the results obtained with the HG phase function and the TPF do not differ appreciably. The average single scattering albedo for cases simulated in Figs. 6(a) and (b) are identical and equal to 0.18 indicating that absorption dominates over scattering. Indeed, Table 1 shows that mass absorption cross-section of *A. variabilis*, $A_{abs,X}$, is about an order of magnitude larger than that of the mass scattering cross-section $S_{sca,X}$. However, for genetically engineered microorganisms with less pigments the absorption cross-section A_{abs,λ_c} decreases and anisotropic scattering effects are expected to be more significant.

Furthermore, Figs. 6(a)–(f) as well as Table 2 show the effects of the presence of the bubbles and different microorganism concentrations on the total local irradiance $G_{PAR}(z)$ and on the penetration depth. They establish that depending on the interfacial area concentration and on the magnitude of the average scattering albedo, ω_{eff}, different scattering phase function approximations can lead to significant differences in the total local irradiance and in the penetration depth. For values of ω_{eff} up to 0.78, the predictions of the penetration depth using the HG and the TPF phase function approximations agree within 5.5% of each other. For $\omega_{\text{eff}} = 0.91$ and 0.97 the relative difference reaches 18.1% and 37.4%, respectively. Moreover, either neglecting in-scattering or assuming isotropic scattering by the bubbles results in underestimation of the penetration depth by as much as 74.1% and 97.2%, respectively, compared with the TPF results. Therefore, for correctly modeling light transfer in bubble sparged photobioreactors, it is necessary to properly approximate the scattering phase function and account for the strongly forward scattering of the bubbles.

Moreover, the presence of bubbles increases the total local irradiance at the surface of the photobioreactor $[G_{PAR}(z = 0)]$ with respect to the total incident irradiance, $G_{PAR,in} = 146.71\ W/m^2$ due to back-scattering. The increase is greater for isotropic scattering than for anisotropic scattering phase functions. For example, in the case of high interfacial area and low microorganism concentration (Fig. 6(e)) the irradiance at the top surface of the reactor is about 79% larger than $G_{PAR,in}$ for the isotropic scattering assumption, 39% larger for the HG phase function, and 3% larger for the TPF. This can be attributed to the fact that bubbles scatter light strongly in the forward direction whereas isotropic scattering equally distributes light in all directions, backward as well as forward. On the other hand, the discrepancy between the HG and the TPF models is due to the over estimation of the back-scattering by the HG as shown in Fig. 5(b).

Finally, let us consider the effect of genetically reducing the pigment content of the microorganisms on the irradiance available to them in the photobioreactor. It is assumed that the same modification performed by Melis et al. [14] on *D. salina* can be performed on *A. variabilis*. In other words, the absorption index of the microorganisms $k_{X,\lambda}$ is reduced by a factor of 10 throughout the PAR. Furthermore, the hypothetical genetically engineered microorganisms are assumed to have the same refractive index as the wild strain. Fig. 7(a) illustrates the scattering phase function of the hypothetical genetically engineered *A. variabilis* obtained with Mie theory along with the HG and TPF approximations. Then, the asymmetry factor g is equal to 0.9931 and the TPF parameters are $f_1 = 0.104$, $h_1 = 0.1$, $\Theta_{\text{cutoff}} = \pi/2$, $g_{TPF,1} = 0.999$, and $g_{TPF,2} = 0.980$. The scattering phase function of the wild strain is reproduced in Fig. 7(b) for comparison. The RTE is solved assuming that the mass scattering cross-section of the microorganisms $S_{sca,X}$ is the same as that of the wild strain whereas the mass absorption cross-section $A_{abs,X}$ decreases also by one order of magnitude. The summary of the radiation characteristics of the hypothetical genetically engineered microorganisms is given in Table 3. The results for the normalized local irradiance using the four

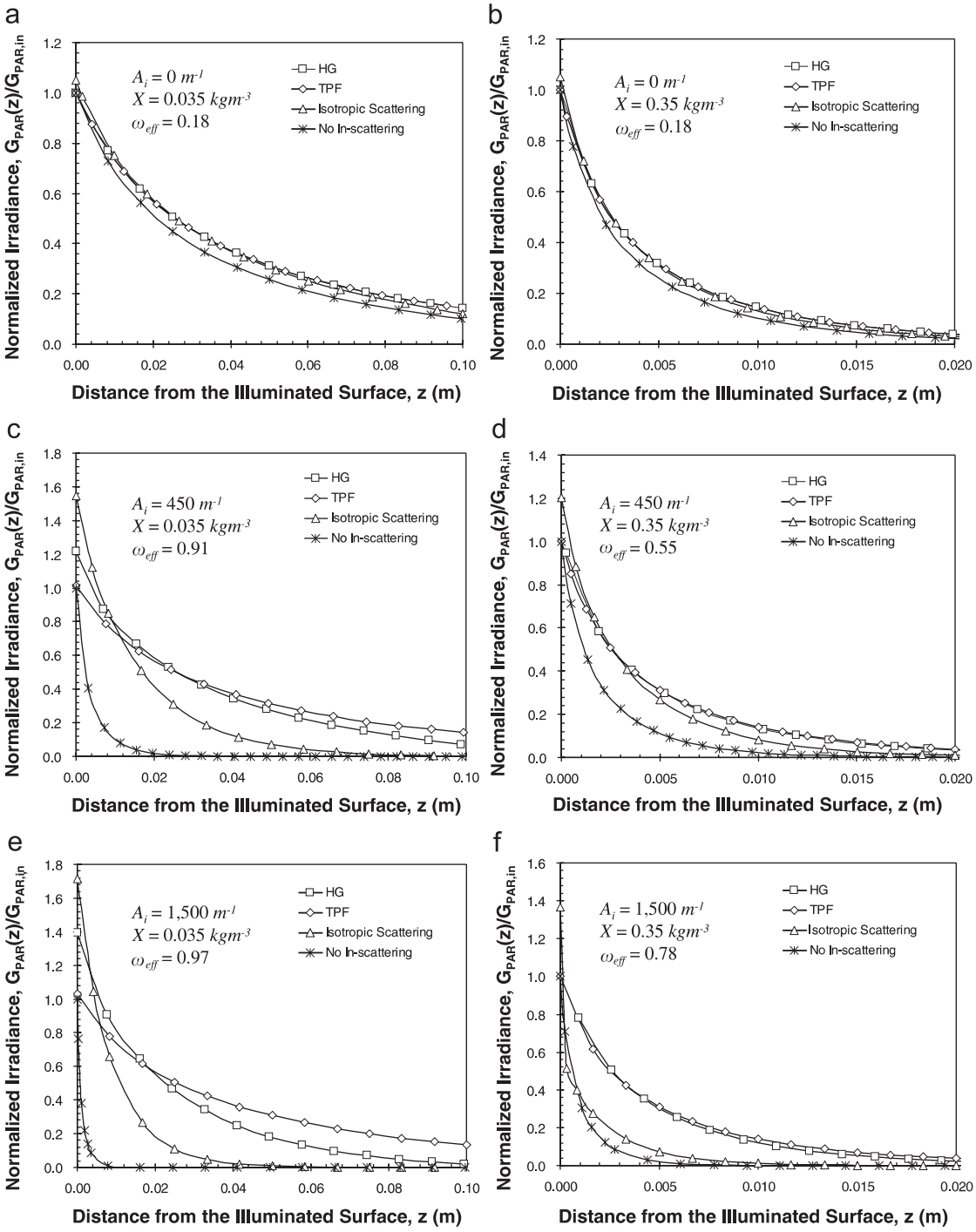

Fig. 6. Normalized local irradiance as a function of the distance from the illuminated surface for interfacial area concentrations: (i) $0\,m^{-1}$; (ii) $450\,m^{-1}$, and (iii) $1,500\,m^{-1}$ and for low ($X = 0.035\,kg\,dry\,cell/m^3$) and high ($X = 0.350\,kg\,dry\,cell/m^3$) bacteria concentrations.

different methods of accounting for scattering are presented in Figs. 7(c) and (d) for the genetically modified strain and the wild strain, respectively for the same bacteria concentration of $0.35\,kg\,dry\,cell/m^3$. The average single scattering albedo, penetration depth, and the percent increase in the total irradiance relative to irradiance at the top surface of the photobioreactor are summarized in Table 4. Because of their reduced pigment content, the genetically engineered microorganisms absorb less light but still scatter it as much as before. For example, for the first box, $\kappa_{eff,434}$ and $\sigma_{eff,434}$ are equal to 14.83 and 24.09, respectively. Thus, absorption no longer dominates over scattering. This is also evident in the value of the average single scattering albedo ω_{eff} which has increased from 0.18 for the wild strain to 0.68 for the genetically engineered microorganisms.

The results establish that for the microorganisms with reduced pigment content, assuming isotropic scattering and ignoring the in-scattering term underestimate the penetration depth

Table 2
Summary of the average single scattering albedo, the penetration depth, and percent increase in the total irradiance relative to irradiance at the top surface of the photobioreactor obtained for various bacteria concentrations and interfacial area concentrations using different scattering models

Fig. 6	Parameters			Penetration depth (mm)				$[G_{PAR}(0) - G_{PAR,in}]/G_{PAR,in}$		
	A_i	X	ω_{eff}	TPF	HG	Iso.	No in-sca.	TPF (%)	HG (%)	Iso. (%)
(a)	Low	Low	0.18	77.5	77.5	73.1	62.8	0	0	5
(b)	Low	High	0.18	7.8	7.8	7.4	6.3	0	0	5
(c)	Medium	Low	0.91	76.8	62.9	32.4	6.3	1	22	55
(d)	Medium	High	0.55	7.6	7.6	6.2	3.3	0	4	20
(e)	High	Low	0.97	75.1	47.0	19.4	2.1	3	39	71
(f)	High	High	0.78	7.6	7.2	2.4	1.6	0	10	37

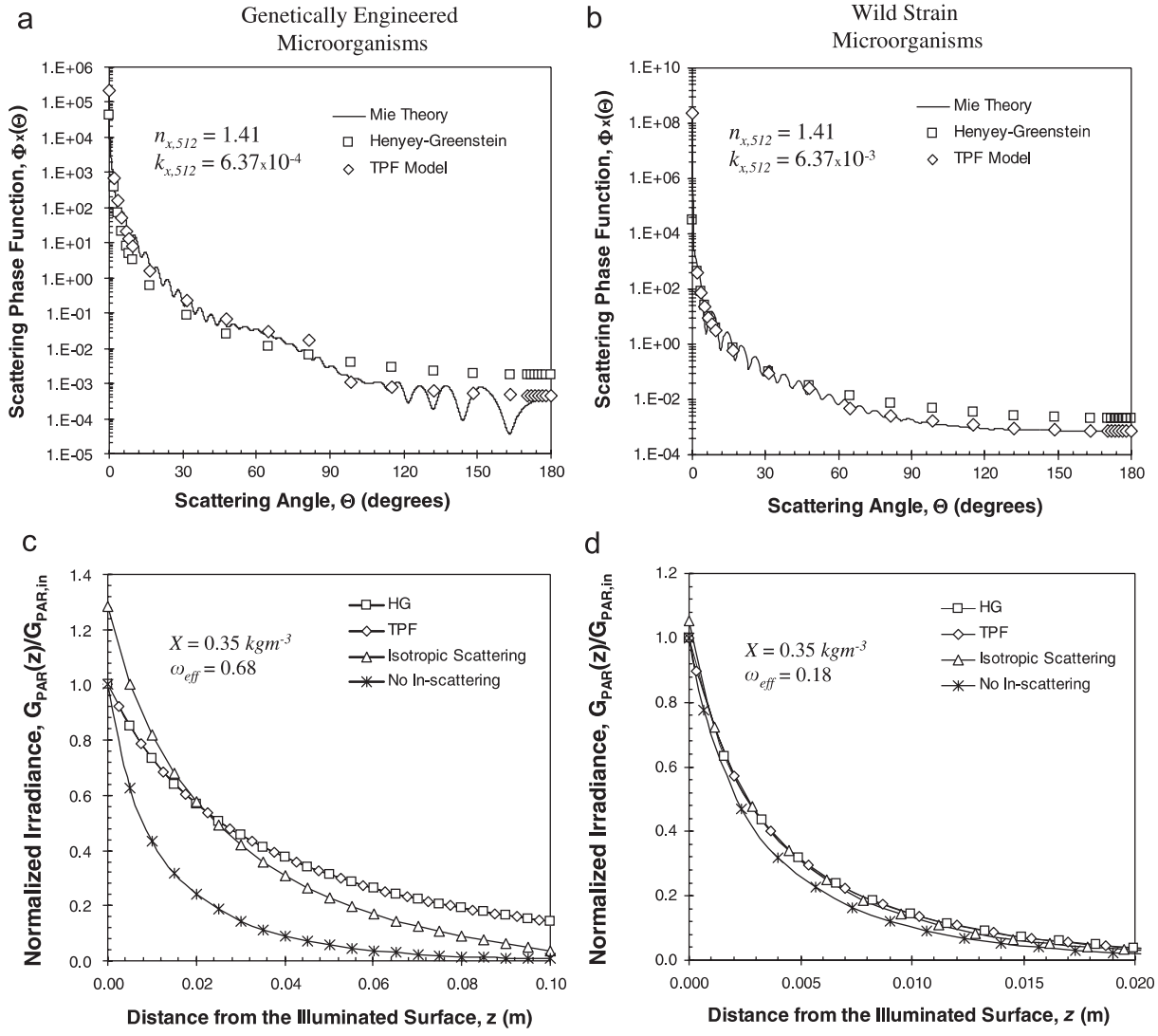

Fig. 7. (a), (b) Scattering phase functions and (c), (d) normalized irradiances for genetically engineered and wild strain of *A. variabilis*, respectively.

by 30% and 70%, respectively. Therefore, unlike for the case of wild strain, it is necessary to account for the anisotropic scattering by the bacteria using either the HG phase function or the TPF. Indeed, the results for either of these scattering phase function approximations do not differ appreciably as shown in Fig. 7(c). Finally, Table 4 indicates that the penetration depth increases almost an order of magnitude from 7.8 to 77.4 mm by reducing the pigment concentration of the microorganisms by one order of magnitude. This can lead to up to 10 fold increase in the overall hydrogen production efficiency of the

Table 3
Summary of the optical properties of hypothetical genetically engineered *A. variabilis*

Box	λ_c (nm)	n_{X,λ_c}	$k_{X,\lambda_c} \times 10^4$	A_{abs,λ_c} (m^2/kg)	S_{sca,λ_c} (m^2/kg)
1	434	1.41	10.09	42.37	68.82
2	512	1.41	6.37	20.99	68.74
3	627	1.41	2.73	31.99	63.57

Table 4
Comparison of the average single scattering albedo, penetration depth and percent increase in the total irradiance relative to irradiance at the top surface of the photobioreactor for the wild and genetically engineered strains of *A. variabilis* at the same bacteria concentration of 0.35 kg dry cell/m^3

Fig. 7	Parameters		Penetration depth (mm)				$[G_{PAR}(0) - G_{PAR,in}]/G_{PAR,in}$		
	Strain type	ω_{eff}	TPF	HG	Iso.	No in-sca.	TPF (%)	HG (%)	Iso (%)
(c)	Wild	0.18	7.8	7.8	7.4	6.3	0	0	5
(d)	Engineered	0.68	77.4	77.4	54.3	23.6	0	0	28

photobioreactors [37] and facilitate scale-up of photobiological hydrogen production processes.

4. Concluding remarks

This manuscript presented modeling of light transfer in a sparged photobioreactor containing gas bubbles and filamentous cyanobacterium *Anabaena variabilis* suspended in water. One-dimensional light transfer modeling was performed by solving the RTE on a spectral basis using the box model and accounting for absorption by both *A. variabilis* and by the liquid phase as well as for anisotropic scattering by the bubbles and the bacteria. A consistent set of radiation characteristics for the bubbles and the microorganisms has been developed from experimental data and from Mie theory. The following conclusions can be drawn:

1. Beer–Lambert's law, i.e., ignoring in-scattering, cannot be applied to predict the irradiance inside the photobioreactor.
2. Isotropic scattering assumption can be used for wild strain microorganisms for practical purposes when there are no bubbles present in the photobioreactor.
3. Anisotropic scattering by the bubbles must be accounted for all bacteria and interfacial area concentrations investigated. This is attributed to the fact that scattering becomes important as the interfacial area concentration increases. Then, the TPF is recommended over the HG phase function as it better approximate the back-scattering.
4. Similarly, anisotropic scattering by the genetically engineered microorganisms with reduced pigmentation should be taken into account. The TPF or the HG phase function gives similar results and the HG phase function is recommended for its simplicity.

Finally, the model presented can be used in conjunction with mass transfer and microorganism growth models to design and optimize the reactor geometry and the sparging conditions for maximum hydrogen production and carbon dioxide consumption by bacteria. It can also be applied to: (i) other types of photosynthetic microorganisms; (ii) different photobioreactor processes such as food product or pharmaceutical production, or (iii) photochemical reactors.

Acknowledgments

The authors gratefully acknowledge the support of the California Energy Commission through the Energy Innovation Small Grant (EISG 53723A/03-29; Project Manager: Michelle McGraw).

References

[1] Das D, Veziroglu TN. Hydrogen production by biological processes: a survey of literature. Int J Hydrogen Energy 2001;26:13–28.
[2] Benemann JR. Hydrogen production by microalgae. J Appl Phycol 2000;12:291–300.
[3] Prince RC, Kheshgi HS. The photobiological production of hydrogen: potential efficiency and effectiveness as a renewable fuel. Crit Rev Microbiol 2005;31:19–31.
[4] Pinto FAL, Troshina O, Lindblad P. A brief look at three decades of research on cyanobacterial hydrogen evolution. Int J Hydrogen Energy 2002;27:1209–15.
[5] Madamwar D, Garg N, Shah V. Cyanobacterial hydrogen production. World J Microbiol Biotechnol 2000;16(8–9):757–67.
[6] Melis A, Zhang L, Forestier M, Ghirardi ML, Seibert M. Sustained photobiological hydrogen gas production upon reversible inactivation of oxygen evolution in the green alga *Chlamydomonas reinhardtii*. Plant Physiol 2000;117:129–39.
[7] Hansel A, Lindblad P. Towards optimization of cyanobacteria as biotechnologically relevant producers of molecular hydrogen, a clean and renewable energy souce. Appl Microbiol Biotechnol 1998;50:153–60.
[8] Hallenbeck PC, Benemann JR. Biological hydrogen production; fundamentals and limiting processes. Int J Hydrogen Energy 2002;27:1185–93.
[9] Melis A, Seibert M, Happe T. Genomics of green algal hydrogen research. Photosynth Res 2004;82:277–88.
[10] Melis A. Green alga hydrogen production: process, challenges and prospects. Int J Hydrogen Energy 2002;27:1217–28.
[11] Happe T, Schutz K, Bohme H. Transcriptional and mutational analysis of the uptake hydrogenase of the filamentous cyanobacterium *Anabaena variabilis* ATCC 29413. J Biotechnol 2000;182:1624–31.

[12] Mikheeva LE, Schmitz O, Shestakov S. Mutants of the cyanobacterium *Anabaena variabilis* altered in hydrogenase activities. Z Naturforsch C 1995;50:505–10.

[13] Sveshnikov DA, Sveshnikova NV, Rao KK, Hall DO. Hydrogen metabolism of mutant forms of *Anabaena variabilis* in continuous cultures and under nutritional stress. FEMS Microbiol Lett 1997;147: 297–301.

[14] Melis A, Neidhardt J, Benemann JR. *Dunaliella salina* (*Chlorophyta*) with small chlorophyll antenna sizes exhibit higher photosynthetic productivities and photon use efficiencies than normally pigmented cells. J Appl Phycol 1999;10:515–25.

[15] Polle JEW, Kanakagiri SD, Melis A. tla1, a DNA insertional transformant of the green alga *Chlamydomonas reinhardtii* with a truncated light-harvesting chlorophyll antenna size. Planta 2003;217:49–59.

[16] Greenbaum E, Blankinship SL, Lee JW, Ford RM. Solar photobiochemistry: simultaneous photoproduction of hydrogen and oxygen in a confined bioreactor. J Phys Chem B 2001;105(17).

[17] Daniel KJ, Laurendeau NM, Incropera FP. Prediction of radiation absorption and scattering in turbid water bodies. J Heat Trans 1979;101:63–7.

[18] Kim BW, Chang HN, Kim IK, Lee KS. Growth kinetics of the photosynthetic bacterium *Chlorobium thiosulfatophilum* in a fed-batch reactor. Biotechnol Bioeng 1992;40:583–92.

[19] Cornet JF, Dussap CG, Dubertret G. A structured model for simulation of cultures of the cyanobacterium *Spirulina platensis* in photobioreactors: I. Coupling between light transfer and growth kinetics. Biotechnol Bioeng 1992;40:817–25.

[20] Cornet JF, Dussap CG, Cluzel P, Dubertret G. A structured model for simulation of cultures of the cyanobacterium *Spirulina platensis* in photobioreactors: II. Identification of kinetic parameters under light and mineral limitations. Biotechnol Bioeng 1992;40:826–34.

[21] Cornet JF, Dussap CG, Gross JB, Binois C, Lasseur C. A simplified monodimensional approach for modeling coupling between radiant light transfer and growth kinetics in photobioreactors. Chem Eng Sci 1995;50:1489–500.

[22] Lee SC. Scattering phase function for fibrous media. Int J Heat Mass Trans 1990;33:2183–90.

[23] Merzlyak MN, Naqvi KR. On recording the true absorption spectrum and scattering spectrum of a turbid sample: application to cell suspensions of cyanobacterium *Anabaena variabilis*. J Photochem Photobiol B 2000;58:123–9.

[24] Latimer P, Eubanks CAH. Absorption spectrophotometry of turbid suspensions: a method of correcting for large systematic deviations. Arch Biochem Biophys 1962;98:274–85.

[25] Stramski D, Mobley CD. Effect of microbial particles on oceanic optics: a database of single-particle optical properties. Limnol Oceanogr 1997;42:538–49.

[26] Pottier L, Pruvost J, Deremetz J, Cornet JF, Legrand J, Dussap CG. A fully predictive model for one-dimensional light attenuation by *Chlamydomonas reinhardtii* in a torous photobioreactor. Biotechnol Bioeng 2005;91:569–82.

[27] Wallis GB. One-dimensional two-phase flow. New York: McGraw-Hill; 1969.

[28] Tien CL, Drolen BL. Thermal radiation in particulate media with dependent and independent scattering. In: Chawla TC, editor, Annual review of numerical fluid mechanics and heat transfer, vol. 1, New York, NY: Hemisphere; 1987, pp. 1–32.

[29] Lee SC. Dependent vs independent scattering in fibrous composites containing parallel fibers. Int J Thermophys Heat Trans 1994;8:641–6.

[30] Modest MF. Radiative heat transfer. San Diego, CA: Academic Press; 2003.

[31] Bohren CF, Huffman DR. Absorption and scattering of light by small particles. New York: Wiley; 1998.

[32] Nicolau VP, Raynaud M, Sacadura JF. Spectral radiative properties identification of fiber insulating materials. Int J Heat Mass Trans 1994;37:311–24.

[33] Hale GM, Querry MR. Optical constants of water in the 200 nm to 200 μm wavelength region. Appl Opt 1973;12:555–63.

[34] Katika KM, Pilon L. Modified method of characteristics for transient radiative transfer. J Quant Spectrosc Radiat Trans 2006;98:220–37.

[35] Baillis D, Pilon L, Randrianalisoa H, Gomez R, Viskanta R. Measurements of radiation characteristics of fused quartz containing bubbles. J Opt Soc Am 2004;21:149–59.

[36] Randrianalisoa H, Baillis D. Pilon L. Improved inverse method for radiative characteristics of closed-cell absorbing porous media, J Thermophys Heat Trans 2006;20:871–83.

[37] Amos WA. Updated cost analysis of photobiological hydrogen production from *Chlamydomonas reinhardtii* green algae. National Renewable Energy Laboratory, NERL/MP-560-35593, 2004.